Journal of Renewable and Sustainable Energy

Radiative cooling resource maps for the contiguous United States

Cite as: J. Renewable Sustainable Energy **11**, 036501 (2019); https://doi.org/10.1063/1.5094510
Submitted: 03 March 2019 . Accepted: 01 June 2019 . Published Online: 25 June 2019

Mengying Li, Hannah B. Peterson, and Carlos F. M. Coimbra

Journal of Renewable and Sustainable Energy ARTICLE scitation.org/journal/rse

Radiative cooling resource maps for the contiguous United States

Cite as: J. Renewable Sustainable Energy **11**, 036501 (2019); doi: 10.1063/1.5094510
Submitted: 3 March 2019 · Accepted: 1 June 2019 ·
Published Online: 25 June 2019

Mengying Li, Hannah B. Peterson, and Carlos F. M. Coimbra[a)]

AFFILIATIONS

Department of Mechanical and Aerospace Engineering, Jacobs School of Engineering, Center of Excellence in Renewable Resource Integration and Center for Energy Research, University of California San Diego, 9500 Gilman Drive, La Jolla, California 92093, USA

[a)]Electronic mail: ccoimbra@ucsd.edu

ABSTRACT

Passive cooling devices take advantage of the partially transparent properties of the atmosphere in the longwave spectral band from 8 to 13 μm (the so-called "atmospheric window") to reject radiation to outer space. Spectrally designed thermophotonic devices have raised substantial attention recently for their potential to provide passive and carbon-free alternatives to air conditioning. However, the level of transparency of the atmospheric window depends on the local content of water vapor in the atmosphere and on the optical depth of clouds in the local sky. Thus, the radiative cooling capacity of solar reflectors not only depends on the optical properties of their surfaces but also on local meteorological conditions. In this work, detailed radiative cooling resource maps for the contiguous United States are presented with the goal of determining the best climates for large-scale deployment of passive radiative cooling technologies. The passive cooling potential is estimated based on ideal optical properties, i.e., zero shortwave absorptance (maximum reflectance) and blackbody longwave emittance. Both annual and season-averaged maps are presented. Daytime and nighttime cooling potential are also computed and compared. The annual average cooling potential over the contiguous United States is 50.5 m^{-2}. The southwestern United States has the highest annual averaged cooling potential, over 70 W m^{-2}, due to its dry and mostly clear sky meteorological conditions. The southeastern United States has the lowest potential, around 30 W m^{-2}, due to frequent humid and/or overcast weather conditions. In the spring and fall months, the Arizona and New Mexico climates provide the highest passive cooling potential, while in the summer months, Nevada and Utah exhibit higher potentials. Passive radiative cooling is primarily effective in the western United States, while it is mostly ineffective in humid and overcast climates elsewhere.

I. INTRODUCTION

Cooling loads for the built environment, including roads, commercial and residential buildings, factories, power plants, and data centers, accounts for a significant portion of the global energy consumption. Commercial buildings consume 40% of total energy in the European Union, with space cooling accounting for nearly half of the total power load.[1] In the United States, about 39% of the total energy consumed was spent on the residential and commercial sectors in 2017, with nearly 15% of the energy consumed for air conditioning purposes.[2,3] Overloaded transformer and transmission line failures due to peak loads during the daytime are often caused by air conditioning demands.[4] Currently, most buildings use reversible heat pumps or powered air conditioning systems with associated high electricity loads for space cooling.[1] A promising technology for reducing the air conditioning load on the grid, especially for locations where the majority the heat load is from solar radiation, is the use of passive radiative cooling devices and paints. These engineered materials are optically selective for reflecting (shortwave) solar radiance while emitting strongly on the (longwave) infrared portion of the electromagnetic spectrum. Passive radiative cooling requires little to no electricity input,[5] and can be deployed in a sustainable way due to modern photonic design of microstructured plastics and selective paints.[6]

The Earth's atmosphere has low absorptivity for electromagnetic waves within the atmospheric window band (longwave, approximately 8–13 μm). Thus, terrestrial objects with high emissivity within the atmospheric window band can be cooled by radiating longwave energy to outer space when directly exposed to the sky. This form of passive cooling is often referred to as "radiative cooling" and has been suggested for nighttime applications.[7–10] In the daytime, even a small value of solar absorptivity will offset the longwave emitting power of the surface, effectively heating the surface. To offset the large cooling demand during the daytime, particularly under direct sunlight,

TABLE I. Summary of the literature related to location specific radiative cooling resources.

Authors	Publish year	Region	Reported parameters	Data duration	Number of locations	Frequency	Contour map
Atwater and Ball[17]	1978	United States	Effective sky temperature and sky temperature depression[a]	1971–1972	11	Seasonal	Y
Exell[18]	1978	Thailand	Sky temperature depression	1969	4	Seasonal	N
Pissimanis and Notaridou[19]	1981	Athens, Greece	Effective sky temperature	1969–1970, 1972–1976	1	Monthly	N
Martin and Berdahl[20]	1984	United States	Sky temperature depression and percentage of hours with sky temperatures below 16 °C	TMY[b]	211	Monthly	Y
Schmetz *et al.*[21]	1986	Europe	Downwelling longwave flux	1981–1982	Satellite	Specific days	Y
Argiriou *et al.*[22]	1994	Athens, Greece	Sky temperature depression	1977–1989	1	Monthly	N
Mahlia *et al.*[23]	2014	Malaysia	Radiative cooling power	2012	10	Monthly	N
Zhang *et al.*[24]	2018	United States	Cooling power	NA	4	Monthly	N
Present work (Li *et al.*)	2019	United States	Radiative cooling resource	2017	1681	Annual, seasonal	Y

[a]The sky temperature depression is the temperature difference between the sky and the surface.
[b]TMY stands for a typical meteorological year.

nanophotonic and polymeric photonic devices have been optically designed recently to exhibit near-zero solar absorptivity while retaining the highly emissive properties in the atmospheric window band.[3,6,11–13]

In addition to the physical constraints for spectral optical properties of surfaces, the heat rejection from passive cooling devices is also limited by local meteorological conditions. The presence of water vapor and clouds increases the emissivity (and the absorptivity) of the atmosphere, with complementary reduction of the transmissivity through the atmospheric window, thus reducing the ability of surfaces to radiate to outer space.[4,14–16] The previous literature on modern radiative cooling devices reports cooling power efficiencies only at one or two testing sites during specific (and short) periods of time. For example, Zhai *et al.*[6] report cooling rate ranges from 100 to 145 W m^{-2} during two clear days in Cave Creek, Arizona, which could only be achieved under cloudless skies with dry atmospheric conditions, based on the analysis performed by Li and Coimbra.[16] For mostly humid and/or frequently cloudy climates, the heat rejection capacity of passive devices is necessarily much lower. Hence, there is a need for radiative cooling resource potential maps in order to proper assess the effectiveness of these passive technologies. As recently pointed out by Vall and Castell,[1] very little research has been directed at evaluating the radiative cooling potential for diverse climates and regions. A summary of studies related to location-specific radiative cooling resources is presented in Table I (including this work for comparison). The literature found on this topic is limited, and none of the previous studies have used extensive and up-to-date meteorological measurements over continental regions.

The main goal of this work is to present radiative cooling resource maps for the contiguous United States (CONUS) and to examine diurnal and seasonal variability in order to propose optimal locations for deployment of passive radiative cooling technologies. Section II presents the theoretical foundations for calculating radiative cooling potentials. Section III presents the methodology for processing the meteorological data used in this work. The passive cooling resource maps are presented in Sec. IV, and conclusions follow in Sec. V.

II. RADIATIVE COOLING VIA THE LONGWAVE ATMOSPHERIC WINDOW

A. Principles of radiative cooling

For a body with temperature T_s facing the open sky (see Fig. 1), the broadband cooling power of the body is

$$q_{\text{cool}}(T_s) = \int_0^{\nu_1} \varepsilon_{s,lw}\left[\pi I_b(\nu, T_s) - J_{\text{sky}}(\nu, T_a)\right] d\nu - \int_{\nu_1}^{\infty} \alpha_{s,sw} q_{\text{sun}}(\nu) d\nu + h_c(T_s - T_a), \quad (1)$$

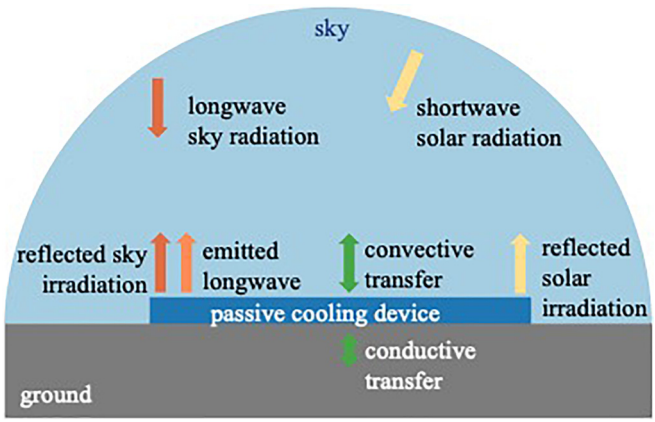

FIG. 1. Schematic of the energy balance for a passive radiative surface under clear sky conditions. With the exception of the direct component of the shortwave solar radiation, all other components and surfaces are assumed to exchange radiation diffusively.

where $\nu_1 = 2500\,\mathrm{cm}^{-1}$ is the wavenumber cutoff between solar shortwave and atmospheric longwave irradiance; $\varepsilon_{s,lw}$ is the monochromatic longwave emittance/absorptance of the body; $I_b(\nu, T_s)$ ($\mathrm{W\,m^{-2}\,sr^{-1}\,cm}$) is the monochromatic blackbody emissive intensity of the body, following Planck's law; J_{sky} (ν, T_a) ($\mathrm{W\,m^{-2}\,cm}$) is the monochromatic sky radiosity at ambient temperature T_a (detailed in Sec. II B); $\alpha_{s,sw}$ is the monochromatic solar shortwave absorptance of the body; q_{sun} (ν) ($\mathrm{W\,m^{-2}\,cm}$) is the spectral solar irradiance on the body, and h_c ($\mathrm{W\,m^{-2}\,K^{-1}}$) is the heat transfer coefficient considering both convective and conductive heat losses.

Figure 2 plots the spectral sky radiosity and solar irradiance for a cloudless atmosphere using previously developed radiative models.[25,26] In the longwave spectrum from 8 to 13 μm, the cloudless atmosphere has a smaller radiosity than the blackbody emissive power of terrestrial objects, making the first term in Eq. (1) positive. Therefore, radiative cooling is mostly via this spectral band, the so-called atmospheric window.

When using spectrally averaged properties, the cooling power is

$$q_{\mathrm{cool}}(T_s) = \bar{\varepsilon}_{s,lw}\left[\sigma T_s^4 - \varepsilon_{\mathrm{sky}}\sigma T_a^4\right] - \bar{\alpha}_{s,sw}G_{\mathrm{sun}} + h_c(T_s - T_a), \quad (2)$$

where $\sigma = 5.67 \times 10^{-8}\,\mathrm{W\,m\,K^{-4}}$ is the Stefan-Boltzmann constant and $\varepsilon_{\mathrm{sky}}$ is the effective emissivity of the sky, which depends on local atmospheric conditions.

To achieve radiative cooling power during both the daytime and the nighttime, radiative coolers need to be highly reflective in the shortwave solar spectrum while highly emissive in the longwave spectrum. For example, Zhai *et al.*[6] developed a material that has a spectrally averaged solar absorptance of 0.04 and a longwave emittance of 0.93. For maximum radiative cooling power, the radiative cooler should have reflectance approaching unity (absorptance approaching zero) in the solar spectrum and emittance approaching unity in the longwave spectrum. In addition, convection and conduction heat loss should be suppressed by means of insulation and/or engineered honeycomb to suppress the onset of fluid motion.[27] Ideally, the maximum cooling power (cooling potential) is

$$q_{\mathrm{cool,ideal}}(T_s) = \sigma T_s^4 - \varepsilon_{\mathrm{sky}}\sigma T_a^4. \quad (3)$$

When the passive cooling surface is kept at temperature $T_s = T_a$ (to further minimize convective and conductive losses), the cooling power flux at the surface is

$$q_{\mathrm{cool,ideal}}(T_a) = \sigma T_a^4(1 - \varepsilon_{\mathrm{sky}}), \quad (4)$$

with cooling power increasing with decreasing values of sky emissivity. The high water vapor content and the presence of clouds tend to increase the sky emissivity (detailed in the Sec. II B), thus decreasing the cooling potential.[16]

B. Atmospheric condition effects

A spectrally resolved two-flux radiative model was developed to compute spectral longwave radiative transfer (wavelength greater than 4 μm) for the earth-atmosphere system under clear skies with different water vapor contents.[25] As shown in Fig. 2, the clear sky has a transparent window from 8 to 13 μm, through which radiative cooling is possible. As discussed above, the transparency of this window decreases with the increasing water vapor content[16] and with the presence of clouds. The model allows us to quantify these effects on the passive cooling potential for ideal surfaces.

Water clouds are modeled using similar methods as used for aerosols. Each water droplet is assumed to have a spherical shape, and thus, the absorption and scattering efficiencies of droplets are calculated using Mie theory results,[25] with the refraction index of water retrieved from the study by Hale and Querry.[28] The absorption and scattering coefficients as well as the asymmetry factors of clouds are further calculated by integrating the efficiencies over a model droplet size distribution.[29] The size distribution of droplets in clouds is assumed to follow a Gamma distribution[30–33]

$$n(r) = r^{1/\sigma_e - 3}\exp\left(-\frac{r}{r_e\sigma_e}\right), \quad (5)$$

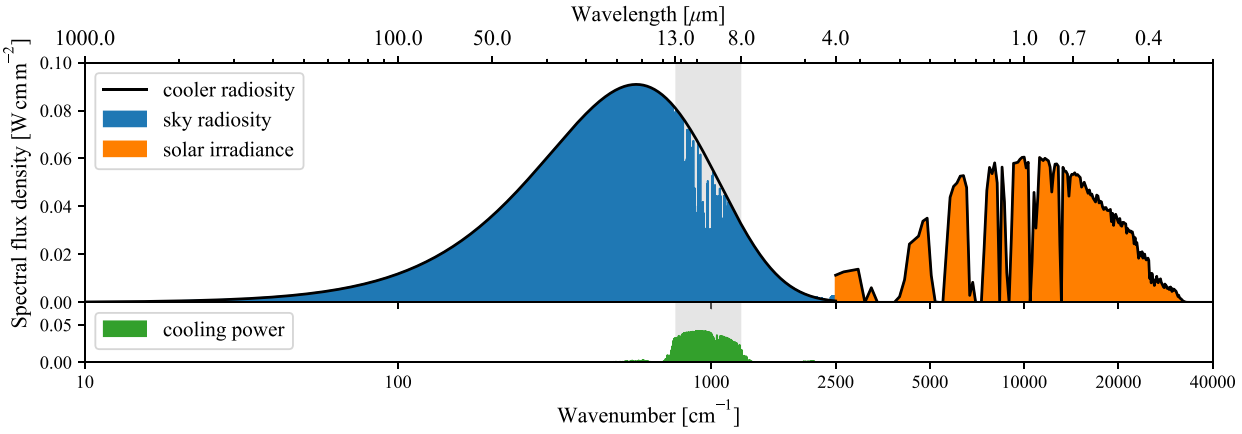

FIG. 2. Model of spectral solar irradiance and sky radiosity under clear skies when ambient temperature $T_a = 294.2$ K, relative humidity $\phi = 70\%$, and solar zenith angle $\theta_z = 30°$.[25,26] The radiosity of an ideal passive cooling device (maximum reflectance for shortwave solar radiation and maximum emittance for longwave radiation) is also shown. The cooling power is shown below within the atmospheric window band of the longwave spectrum. For clarity of display, longwave power flux density is scaled down by a factor of 5.

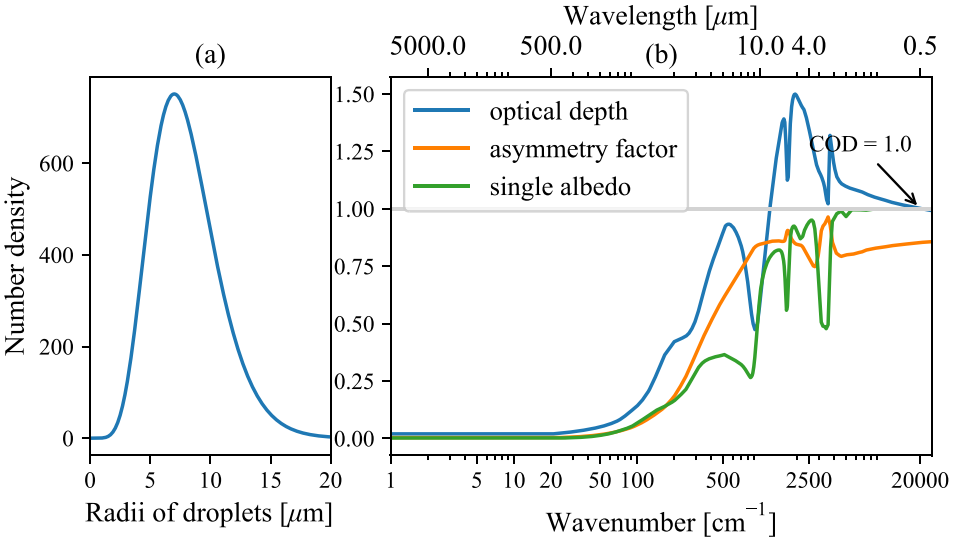

FIG. 3. (a) Size distribution of droplets in the model clouds for $r_e = 10\,\mu$m. (b) Spectral optical depth, single albedo, and asymmetry factor of model clouds for unity value of COD. The subscript 497.5 nm is omitted in the text for clarity.

where r_e and σ_e are the mean effective radius and variance, respectively. Here, we assume the mean effective radius of $r_e = 10.0\,\mu$m and $\sigma_e = 0.1$, as suggested in the studies by Barker *et al.* and Walther *et al.* and used in several geoestationary satellite products.[32,33] Miles *et al.* suggested that an effective radius of 5.4 μm may better represent continental clouds. We use the smaller effective radius distribution to assess the uncertainty of the modeled cooling potential (see Fig. 5). The spectral dispersion k often used to represent the spread of the droplet size (instead of σ_e) is defined as $k = (1/\sigma_e - 2)^{-1/2}$. When $\sigma_e = 0.1$, $k = 0.354$, which is a typical value for both marine and continental clouds.[31] The size distribution of water droplets is shown in Fig. 3(a).

Clouds are considered as layers with a predefined Cloud Optical Depth (COD) at 497.5 nm defined as COD $= \kappa_{e,\mathrm{cld}}\,\Delta H_c$, where $\kappa_{e,\mathrm{cld}}$ (cm^{-1}) is the extinction coefficient of clouds and ΔH_c (cm) is the thickness of clouds. The spectral optical depth, single albedo, and asymmetry factors of clouds are shown in Fig. 3(b) for COD = 1.0.

The extinction coefficient, single albedo, and asymmetry factor of each atmospheric layer containing clouds are

$$\begin{aligned} \kappa_e &= \kappa_{e,\mathrm{gas}} + \kappa_{e,\mathrm{aer}} + \kappa_{e,\mathrm{cld}}, \\ \tilde{\rho} &= \frac{\kappa_{s,\mathrm{aer}} + \kappa_{s,\mathrm{cld}}}{\kappa_e}, \\ e_g &= \frac{e_{g,\mathrm{aer}}\kappa_{s,\mathrm{aer}} + e_{g,\mathrm{cld}}\kappa_{s,\mathrm{cld}}}{\kappa_{s,\mathrm{aer}} + \kappa_{s,\mathrm{cld}}}, \end{aligned} \tag{6}$$

where the asymmetry factor e_g is the weighted sum for the mixture of aerosols and clouds using scattering coefficients as the weights. The scattering is then treated as isotropic using the δ-M scaling method,[34] and the monochromatic fluxes are solved using the procedures outlined in the study by Li *et al.*[25]

For partly cloudy skies, the spectral downwelling longwave irradiance (sky radiosity) calculated from the model is expressed as

$$J_{\mathrm{sky}}(\nu, T_a) = J_{\mathrm{sky},c}(\nu, T_a)(1 - \mathrm{CF}) + J_{\mathrm{sky},oc}(\nu, T_a)\mathrm{CF}, \tag{7}$$

where ν is the wavenumber (cm^{-1}), T_a (K) is the ambient air temperature at the screening level (10 m above the surface), CF is the cloud fraction, and the subscripts "c" and "oc" represent the clear skies and overcast skies, respectively. Then, the spectral cooling power of an ideal cooler at ambient temperature is calculated from Eqs. (1) to (4). Figure 4 shows the spectral longwave cooling power for $T_s = T_a = 294.2$ K and $\phi = 70\%$. Clearly, the cooling power decreases when more clouds are present in the atmosphere because clouds also "block" the atmospheric window. Figure 5 shows the broadband cooling potential with respect to both COD and cloud base temperature (CBT) when CF = 1.0. The ambient is at 294.2 K and $\phi = 70\%$. The cooling power for clear skies at the nominal conditions described above is 71.9 W m^{-2} for the Air Force Geophysics Laboratory (AFGL) midlatitude summer temperature profile, and it decreases with increasing COD and CBT. Different temperature profiles (corrected to match the ambient conditions) introduce less than 5 W m^{-2} deviations to the cooling power potential. When the effective radius of clouds is assumed to be 5.4 μm, the cooling power is increased by less than 10 W m^{-2} when compared to the cooling power calculated with $r_e = 10\,\mu$m.

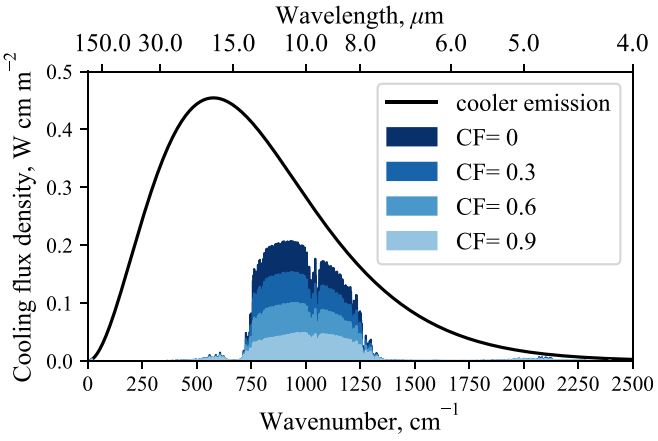

FIG. 4. Spectral longwave cooling power with respect to the cloud fraction under partly cloudy skies when ambient temperature $T_a = 294.2$ K and $\phi = 70\%$. Model clouds are assumed to have a base height of 0.54 km, a thickness of 0.44 km, and an optical depth of 5.0 at 497.5 nm.

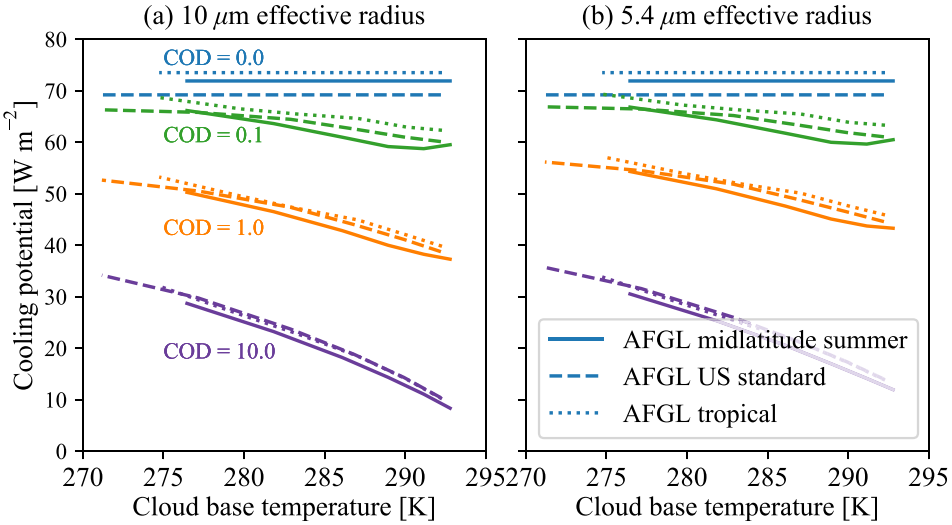

FIG. 5. Broadband cooling potential for different cloud base temperatures and cloud optical depths when ambient $T_a = 294.2$ K, $\phi = 70\%$, and the cloud fraction is 1.0. Panel (a) shows the results for model clouds' effective radius r_e equal to 10 μm, while panel (b) shows results for r_e equal to 5.4 μm. Cooling potentials for different temperature profiles are also plotted for comparison.

If detailed atmosphere temperature, pressure, and concentration vertical profiles are specified, the sky radiosity can be calculated precisely using the radiative transfer model. If only ambient temperature and relative humidity are given, empirical expressions of effective sky emissivity can be used. The empirical all-sky effective emissivity of the sky for the contiguous United States has been recently determined to be[35]

$$\begin{aligned} \varepsilon_{\text{sky}} &= \varepsilon_{\text{sky,c}}(1 - 0.78\,\text{CF}) + 0.38\,\text{CF}^{0.95}\phi^{0.17}, \\ \varepsilon_{\text{sky,c}} &= 0.618 + 0.056\sqrt{P_w}, \end{aligned} \tag{8}$$

where $\varepsilon_{\text{sky,c}}$ is the effective sky emissivity under clear skies, ϕ is the ambient relative humidity, and P_w (Pa) is the ambient water vapor partial pressure. From local measurements of ambient temperature, relative humidity (or dew point), and cloud fraction, the effective sky emissivity and radiative cooling potentials can be calculated. The mean bias error found by using Eq. (8) to estimate the Downwelling Longwave Flux (DLW) is $-4.94\,\text{W m}^{-2}$ (Ref. 35), which implies that the uncertainty in estimating seasonally and annually averaged cooling potentials is of the order of $5\,\text{W m}^{-2}$.

III. PROCESSING OF METEOROLOGICAL DATA

A. Data retrieval

Local meteorological measurements were retrieved from the National Oceanic and Atmospheric Administration (NOAA) Automated Surface Observing System (ASOS) network via direct File Transfer Protocol (FTP) access.[36] A total of 1681 stations across the contiguous United States were used to collect data for the year 2017 (see Fig. 6 for the spatial distribution of the stations). Most stations considered in this work reported a full year worth of data, with some reporting incomplete or low quality data periods, and those periods were removed from consideration.

Each station records intra-hour measurements of meteorological variables, including air temperature (T_a), dew point (T_d), and cloud fraction (CF). Only measurements designated as having passed all quality control checks (based on QC codes provided by ASOS) were used. ASOS data have multiple entries of cloud fraction values based on cloud types, and the CF values used in this work are the average of all entries.

From air temperature T_a and dew point T_d, the water vapor partial pressure P_w and relative humidity ϕ are calculated using Magus-like expressions[37]

$$\begin{aligned} P_w &= P_0 \quad \exp\left(\frac{c_T T_d}{T_d + T_0}\right) \\ \phi &= \frac{P_w}{P_0 \quad \exp\left(\frac{c_T T_a}{T_a + T_0}\right)}, \end{aligned} \tag{9}$$

where $P_0 = 610.94\,\text{Pa}$, $c_T = 17.625$, and $T_0 = 243.04\,^\circ\text{C}$. Note that in the above two equations, temperatures T_a and T_d have units of degrees Celsius.

The radiative cooling potential is then calculated from T_a, P_w, ϕ, and CF using Eqs. (4) and (8) for each entry. Data are separated into the four seasons according to the timestamps of the entries. Timestamps are also used to calculate the solar zenith angles of the entries to separate them into daytime or nighttime periods. Clear sky periods are determined when the cloud fraction equals zero. With this, the overall annual, annual daytime, and nighttime and seasonal averages of radiative cooling potential across CONUS are computed and interpolated for mapping.

B. Spatial mapping

An inverse distance weighting (IDW) spatial interpolation methodology is used to derive variables (air temperature, water vapor partial pressure, and ratio of clear sky period and cooling potential) in order to form a uniform latitude-longitude grid. The variable values for nonstation locations are interpolated using values from all stations[38]

$$\hat{Z} = \frac{\sum_{i=1}^{N} w(d_i) Z_i}{\sum_{i=1}^{N} w(d_i)}, \tag{10}$$

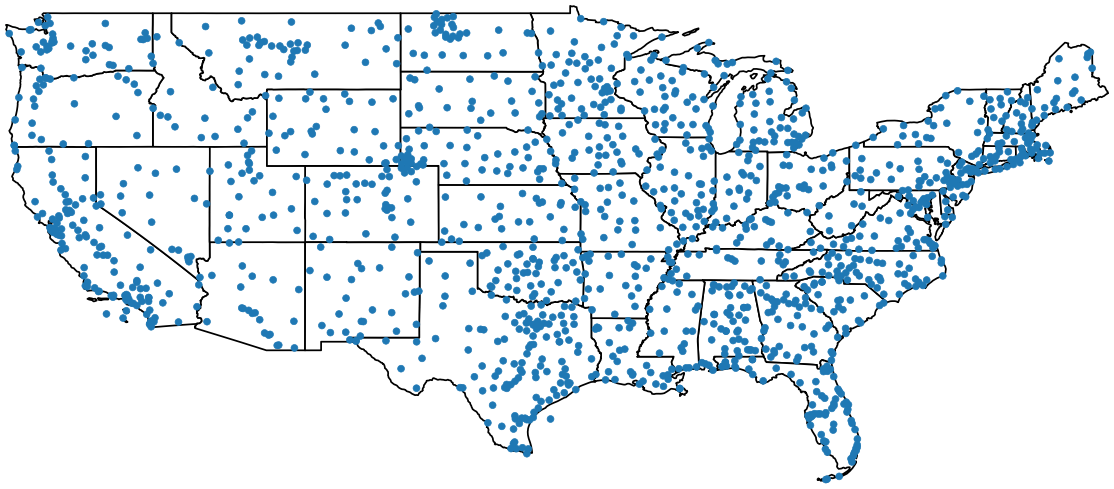

FIG. 6. Location of the 1681 ASOS stations used in this work.

where N is the number of stations; d_i is the geographic distance between a station i and the current location; Z_i is the variable value at a station i, and $w(d_i)$ are weighting functions that inversely depend on d

$$w(d) = \frac{1}{d^p}, \tag{11}$$

where p is a positive power factor set to unity in this work.

After the IDW interpolation, 2-dimensional gradients at each grid point are calculated according to latitude and longitude values to determine the degree of similarity to adjacent points. Extreme (top 2%) gradients are interpreted as resulting from potentially faulty data. These outliers are replaced with averages for adjacent points.

IV. RESULTS AND DISCUSSION

Table II presents the spatial range and mean of annually and seasonally averaged ambient temperature T_a, water vapor partial pressure P_w, and ratio of clear sky periods R_c and radiative cooling potential $q_{\text{cool,ideal}}$ over the contiguous United States (CONUS). The average radiative cooling potential for the entire CONUS area is 50.5 W m^{-2}.

The total area of CONUS can be divided into four census regions: the West, Midwest, South, and Northeast.[39] The following

TABLE II. Range and mean of annually and seasonally averaged T_a, P_w, R_c, and $q_{\text{cool,ideal}}$ over the contiguous United States.

	Annual	Spring (MAM)	Summer (JJA)	Fall (SON)	Winter (DJF)	Annual daytime	Annual nighttime
Air temperature T_a (°C)							
Minimum	4.2	4.3	18.2	5.3	−8.6	8.0	0.4
Maximum	23.5	23.2	28.7	24.1	18.7	25.5	21.4
Mean	14.3	14.0	23.7	15.0	5.0	17.4	11.2
Water vapor pressure P_w (Pa)							
Minimum	578.3	555.2	909.1	535.6	300.1	626.0	515.9
Maximum	2262.5	1992.5	2889.9	2442.4	1683.5	2342.2	2195.6
Mean	1279.4	1143.7	1915.7	1301.9	769.2	1341.2	1213.9
Ratio of clear sky periods R_c							
Minimum	0.27	0.24	0.28	0.32	0.21	0.24	0.31
Maximum	0.67	0.72	0.77	0.74	0.63	0.65	0.70
Mean	0.47	0.44	0.52	0.51	0.42	0.43	0.50
Cooling potential $q_{\text{cool,ideal}}$ (W m^{-2})							
Minimum	32.2	34.6	19.9	27.8	36.9	31.5	33.0
Maximum	80.3	89.7	87.6	83.6	73.9	85.6	75.1
Mean	50.5	52.8	48.2	52.1	49.7	52.7	48.3

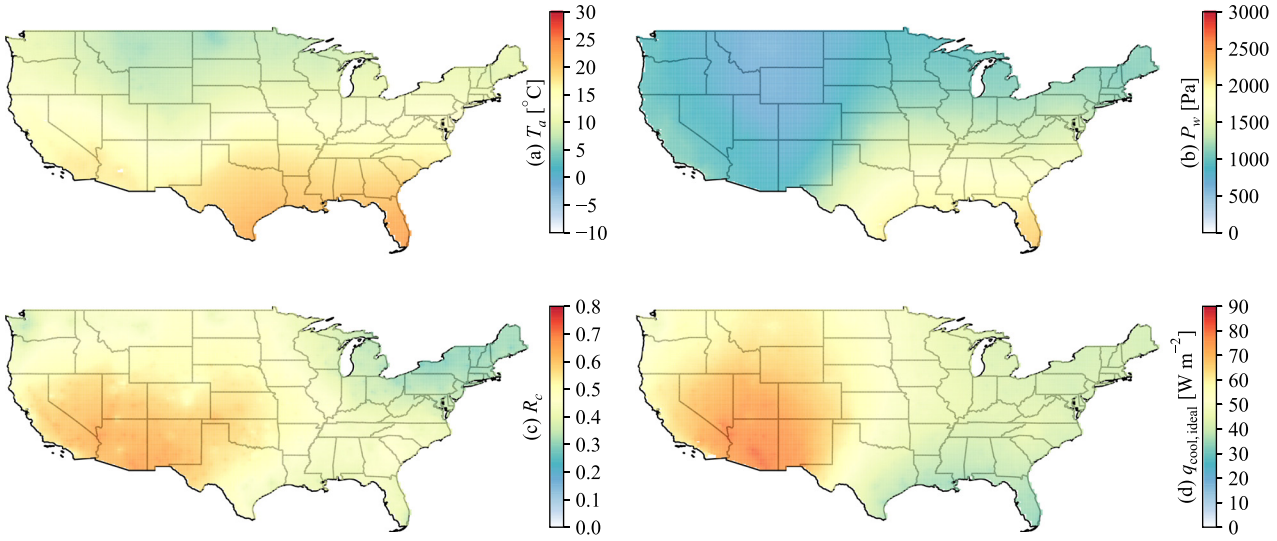

FIG. 7. Map of annual average values for: (a) air temperature T_a, (b) water vapor partial pressure P_w, (c) ratio of clear sky periods R_c, and (d) radiative cooling potential $q_{cool,ideal}$.

discussion uses this common geographic division when referring to specific regions.

A. Annual average resource

Figure 7 shows a map of annually averaged T_a, P_w, R_c, and $q_{cool,ideal}$. Temperature decreases with the increasing latitude. The West is the driest as indicated by P_w, while the South is more humid. The Southwest has over 50% clear sky periods throughout the year, while the Southeast has less than 30%. Since radiative cooling is most effective in dry and cloudless conditions, the Southwest has an annual average radiative cooling potential of over 70 W m^{-2}. The other regions have lower than 50 W m^{-2} cooling potential, with the South having the lowest. Note that the cooling potential is the maximum possible cooling rate under given meteorological conditions. Absorption of solar irradiance and convective and conductive heat loss all reduce the cooling rate of radiative coolers as they operate.

B. Diurnal variations

Figures 8 and 9 show the maps of annually averaged variables during the daytime and nighttime, respectively. The water vapor partial pressure and ratio of clear sky periods show little diurnal variation, while ambient temperature is around 6 °C higher during the day. Therefore, the cooling potential is around 5 W m^{-2} higher during the day than the night, which matches the cooling demands for most residential and commercial buildings. According to the longwave irradiance distribution within the atmosphere,[16] ambient air is primarily

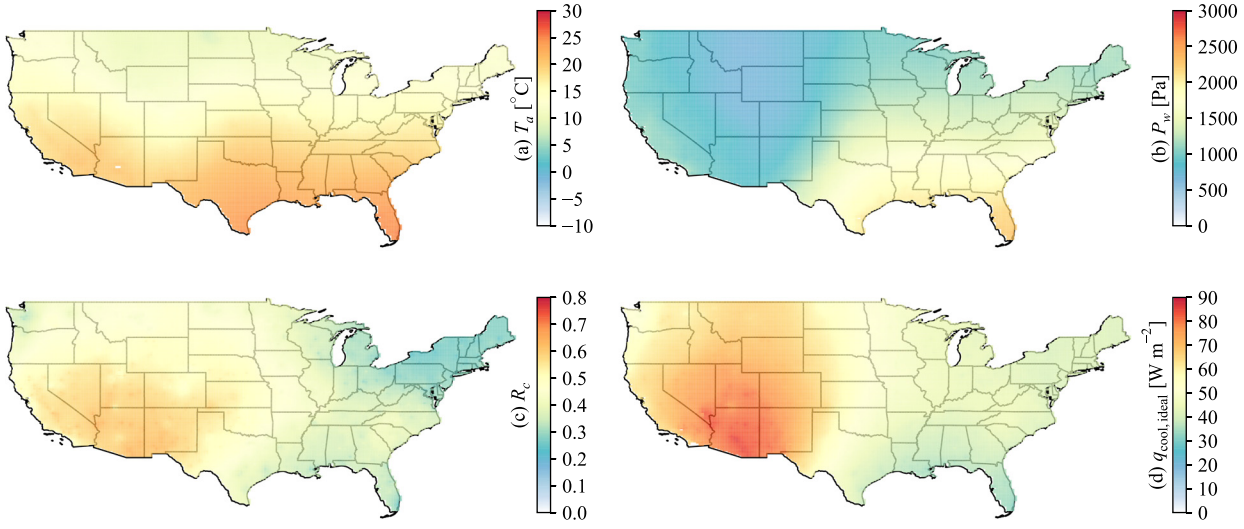

FIG. 8. Annual average values during the daytime. From top left, clockwise: (a) air temperature T_a, (b) water vapor partial pressure P_w, (c) ratio of clear sky periods R_c, and (d) radiative cooling potential $q_{cool,ideal}$.

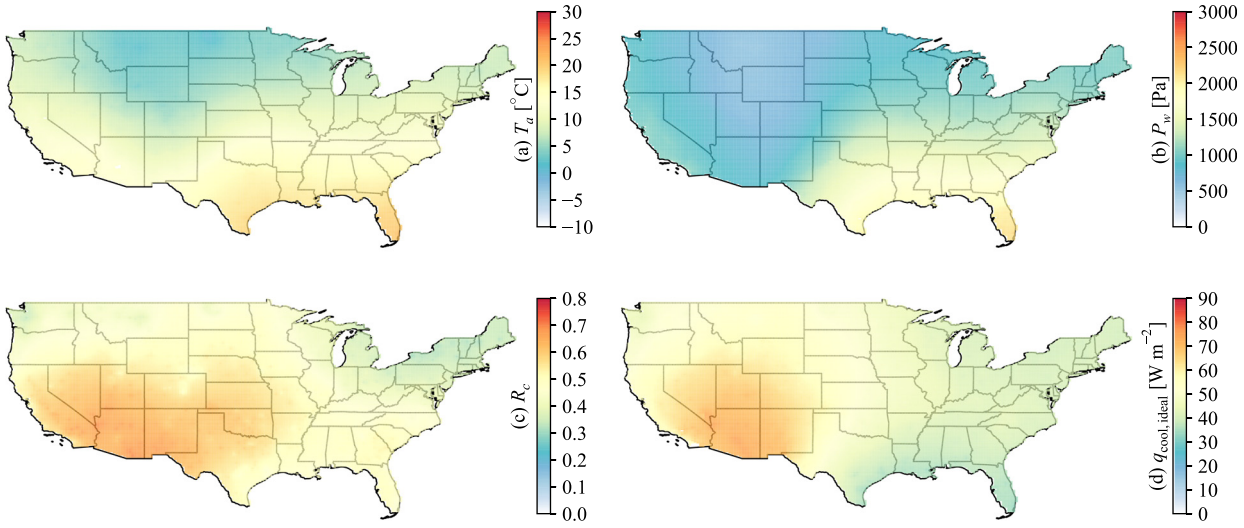

FIG. 9. Annual average values during the nighttime. From top left: (a) air temperature T_a, (b) water vapor partial pressure P_w, (c) ratio of clear sky periods R_c, and (d) radiative cooling potential $q_{cool,ideal}$.

heated by the Earth's surface, which itself is heated by absorbing solar irradiance during the day. If the ground is covered by passive coolers (objects highly reflective in the solar spectrum), the ambient air is heated to a lesser degree, reducing the ambient temperature during the day. With this, the deployment of passive coolers decreases diurnal variations in temperature.

C. Seasonal variations

Figures 10–13 show maps of seasonally averaged variables in the spring (March-April-May), summer (June-July-August), fall (September-October-November), and winter (December-January-February). Duringthe spring, Arizona and New Mexico experience dry and generally cloudless weather, yielding a high cooling potential of around 80 W m^{-2}. California, Nevada, Utah, and Colorado have potentials around 60–70 W m^{-2}. The ambient temperature for the above-mentioned states is around 10–15 °C such that radiative cooling is expected to fulfill most of the cooling demands from residential sectors. In contrast, the South has an ambient temperature of around 20 °C and a cooling potential of around 40–50 W m^{-2} such that additional methods of cooling are necessary. During the summer, the West is dry and mostly clear, yielding a cooling potential above 70 W m^{-2}. Nevada and Utah have the highest potential of around 80 W m^{-2}. The South experiences generally humid and cloudy summers, with a low cooling potential of around 30 W m^{-2}. Therefore, radiative cooling during the summer

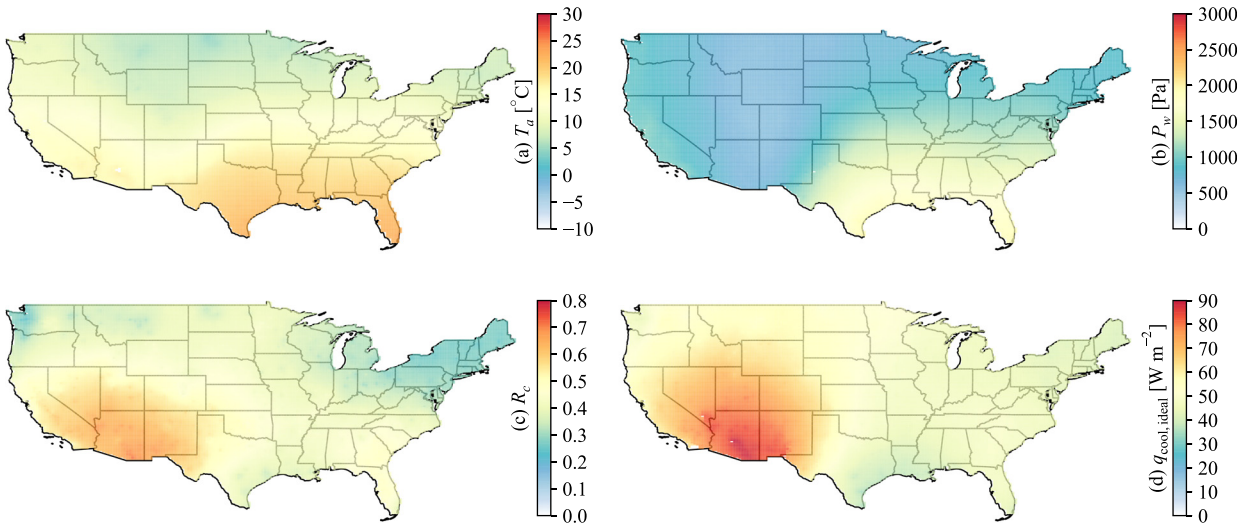

FIG. 10. From top left: (a) air temperature T_a, (b) water vapor partial pressure P_w, (c) ratio of clear sky periods R_c, and (d) radiative cooling potential $q_{cool,ideal}$ for the spring months (March-April-May).

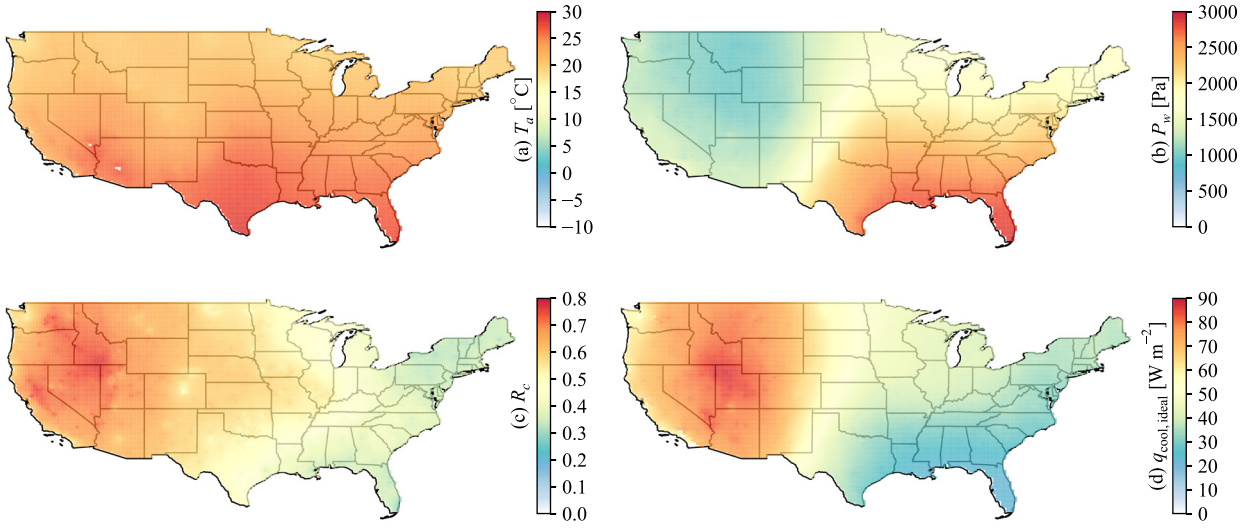

FIG. 11. From top left: (a) air temperature T_a, (b) water vapor partial pressure P_w, (c) ratio of clear sky periods R_c, and (d) radiative cooling potential $q_{cool,ideal}$ for the summer months (June-July-August).

is most promising in the West. During the fall, the spatial distribution of radiative cooling potential is similar to that in the spring, with radiative cooling being effective primarily in the Southwest. During the winter, the water vapor content in the atmosphere (represented by P_w) is low due to lower air temperature. Consequently, the Southwest has a cooling potential of around 60 W m^{-2}, while other regions have potentials of around 40–50 W m^{-2}. To prevent unnecessary cooling and/or the coolers from icing over during the winter, they should be covered.

V. CONCLUSIONS

Radiative coolers are optically designed to reject heat to outer space through the longwave atmospheric window spectral band (8–13 μm). The cooling rates of radiative coolers are found to be dependent not only on their optical properties but also on local meteorological conditions. The presence of water vapor and clouds reduces the "transparency" of the atmospheric window, thus reducing the cooling potential (capability) of the coolers. This work presents radiative cooling resource (potential) maps for the contiguous United States to assist in the design and deployment of such cooling devices. The cooling potential of a cooler is defined to be its maximum possible cooling rate, assuming its optical properties are ideal and neglecting convective/conductive heat losses. For real (nonideal) surfaces, the cooling power is smaller than the estimates in this work due to nonzero solar absorption, nonblackbody longwave emissive power, and nonzero convective heating. Therefore, the estimates in this work

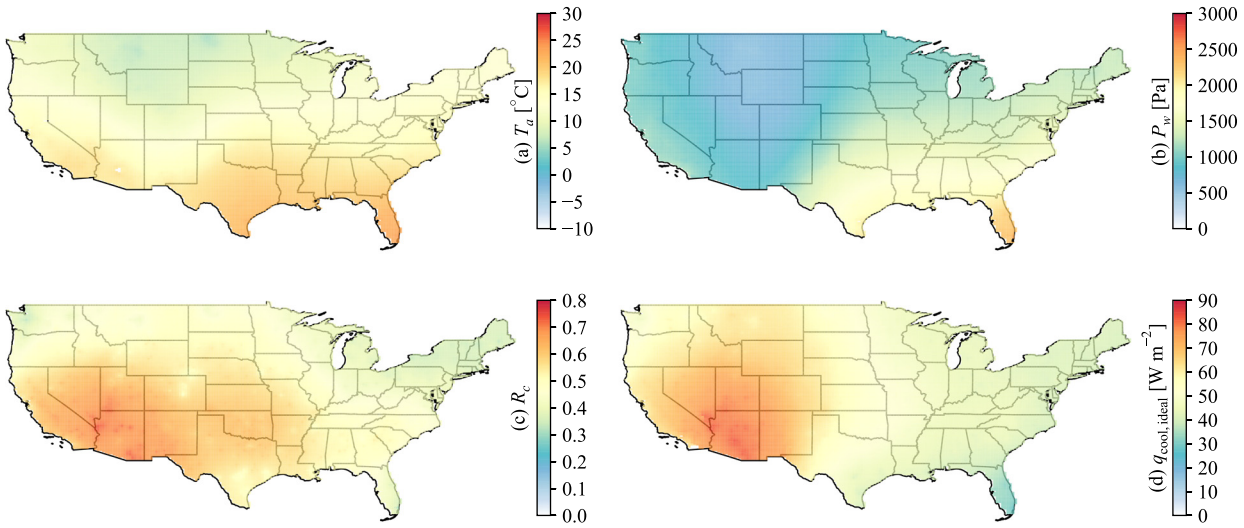

FIG. 12. From top left: (a) air temperature T_a, (b) water vapor partial pressure P_w, (c) ratio of clear sky periods R_c, and (d) radiative cooling potential $q_{cool,ideal}$ for the fall months (September-October-November).

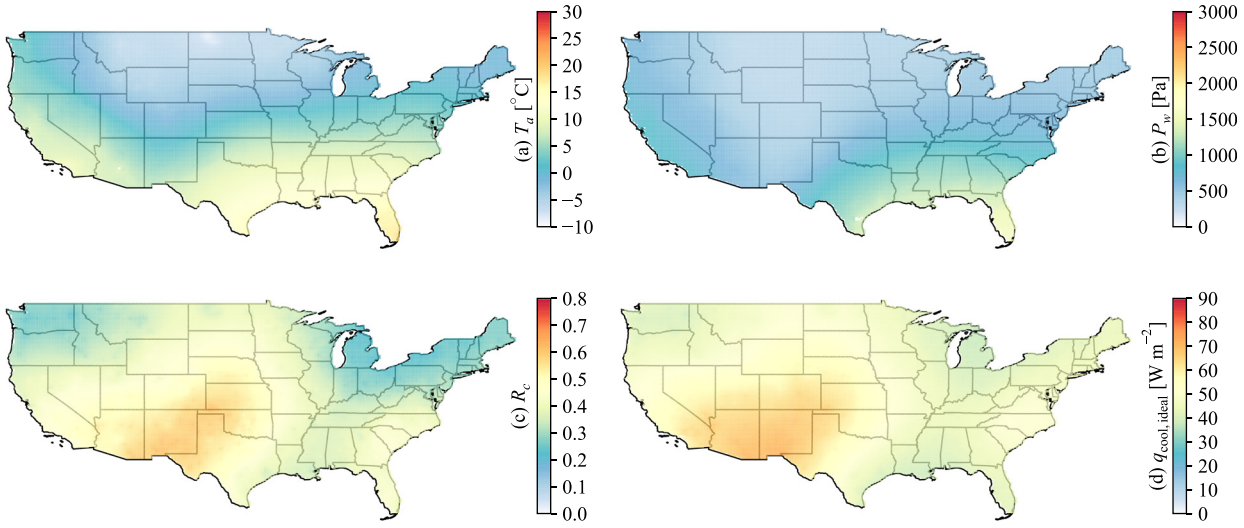

FIG. 13. From top left: (a) air temperature T_a, (b) water vapor partial pressure P_w, (c) ratio of clear sky periods R_c, and (d) radiative cooling potential $q_{cool,ideal}$ for the winter months (December-January-February).

represent upper bounds for passive cooling rates. It is also relevant to note that the radiative cooling resource maps for the contiguous United States presented here are generated using extensive meteorological data collected from 1681 weather stations over the entire year of 2017. Diurnal and seasonal variations of cooling potentials are also analyzed below.

Annually, the Southwestern United States is dry and mostly clear, resulting in an average radiative cooling potential of over 70 W m^{-2} and making it the region where radiative cooling is most effective. In contrast, the South has the lowest cooling potential of around 30 W m^{-2} due to local humid and cloudy meteorological conditions. Convective/conductive heat loss and/or as little as 5% solar irradiance absorption lead to ineffective radiative cooling in the South. Additionally, the water vapor content in the atmosphere and clearness of the sky are weaker functions of time of day, as opposed to ambient air temperature, which is always higher during the day. Therefore, cooling potentials are around 5 W m^{-2} higher during the daytime than during the nighttime.

For the spring (March-April-May) and fall (September-October-November), Arizona and New Mexico exhibit cooling potentials around 80 W m^{-2}, due to dry and cloudless conditions. Surrounding states such as California, Nevada, Utah, and Colorado have potential ranging from 60 to 70 W m^{-2}. Other states exhibit cooling potentials about 10 W m^{-2} lower. During the summer, the entire West reaches cooling potential values over 70 W m^{-2}, again due to high ambient temperatures, low humidities, and clear skies. The South, in contrast, has a cooling potential lower than 40 W m^{-2} due to humid and cloudy summer climate. Most regions of CONUS during the winter are generally dry and clear, with cooling potentials of around 50 W m^{-2}. To prevent over-cooling and/or icing during colder weather, cooling devices must be properly stored or covered, which also diminishes their range of practical applications.

In summary, passive radiative cooling has much potential in the western region of CONUS, due to the prevalent hot and dry weather in the region. Just as with swamp or evaporative coolers, but due to different physical mechanisms, the effectiveness of passive radiative cooling devices is greatly reduced for hot and humid conditions. Unfortunately, those are the conditions that often demand very high power loads for air conditioning.

ACKNOWLEDGMENTS

The authors gratefully acknowledge partial support of the U.S. Department of Energy's Office of Energy Efficiency and Renewable Energy (EERE) under Solar Energy Technologies Office (SETO) Agreement No. EE0008216.

REFERENCES

[1]S. Vall and A. Castell, "Radiative cooling as low-grade energy source: A literature review," Renewable Sustainable Energy Rev. **77**, 803–820 (2017).
[2]U.S. Energy Information Administration, *How Much Energy is Consumed in U.S. Residential and Commercial Buildings?* (U.S. Energy Information Administration, 2018).
[3]A. P. Raman, M. A. Anoma, L. Zhu, E. Rephaeli, and S. Fan, "Passive radiative cooling below ambient air temperature under direct sunlight," Nature **515**, 540 (2014).
[4]X. Lu, P. Xu, H. Wang, T. Yang, and J. Hou, "Cooling potential and applications prospects of passive radiative cooling in buildings: The current state-of-the-art," Renewable Sustainable Energy Rev. **65**, 1079–1097 (2016).
[5]P. Berdahl, M. Martin, and F. Sakkal, "Thermal performance of radiative cooling panels," Int. J. Heat Mass Transfer **26**, 871–880 (1983).
[6]Y. Zhai, Y. Ma, S. N. David, D. Zhao, R. Lou, G. Tan, R. Yang, and X. Yin, "Scalable-manufactured randomized glass-polymer hybrid metamaterial for daytime radiative cooling," Science **355**, 1062–1066 (2017).
[7]S. Catalanotti, V. Cuomo, G. Piro, D. Ruggi, V. Silvestrini, and G. Troise, "The radiative cooling of selective surfaces," Sol. Energy **17**, 83–89 (1975).
[8]J. André and L. Mahrt, "The nocturnal surface inversion and influence of clear-air radiative cooling," J. Atmos. Sci. **39**, 864–878 (1982).
[9]U. Eicker and A. Dalibard, "Photovoltaic–thermal collectors for night radiative cooling of buildings," Sol. Energy **85**, 1322–1335 (2011).
[10]M. M. Hossain and M. Gu, "Radiative cooling: Principles, progress, and potentials," Adv. Sci. **3**, 1500360 (2016).

[11]E. Rephaeli, A. Raman, and S. Fan, "Ultrabroadband photonic structures to achieve high-performance daytime radiative cooling," Nano Lett. **13**, 1457–1461 (2013).
[12]Z. Huang and X. Ruan, "Nanoparticle embedded double-layer coating for daytime radiative cooling," Int. J. Heat Mass Transfer **104**, 890–896 (2017).
[13]M. Zeyghami, D. Y. Goswami, and E. Stefanakos, "A review of clear sky radiative cooling developments and applications in renewable power systems and passive building cooling," Sol. Energy Mater. Sol. Cells **178**, 115–128 (2018).
[14]A. Harrison, "Effect of atmospheric humidity on radiation cooling," Sol. Energy **26**, 243–247 (1981).
[15]C. Tso, K. Chan, and C. Y. Chao, "A field investigation of passive radiative cooling under Hong Kong's climate," Renewable Energy **106**, 52–61 (2017).
[16]M. Li and C. F. M. Coimbra, "On the effective spectral emissivity of clear skies and the radiative cooling potential of selectively designed materials," Int. J. Heat Mass Transfer **135**, 1053–1062 (2019).
[17]M. A. Atwater and J. T. Ball, "Computation of IR sky temperature and comparison with surface temperature," Sol. Energy **21**, 211–216 (1978).
[18]R. Exell, "The atmospheric radiation climate of Thailand," Sol. Energy **21**, 73–79 (1978).
[19]D. Pissimanis and V. Notaridou, "The atmospheric radiation in Athens during the summer," Sol. Energy **26**, 525–528 (1981).
[20]M. Martin and P. Berdahl, "Characteristics of infrared sky radiation in the United States," Sol. Energy **33**, 321–336 (1984).
[21]P. Schmetz, J. Schmetz, and E. Raschke, "Estimation of daytime downward longwave radiation at the surface from satellite and grid point data," Theor. Appl. Climatol. **37**, 136–149 (1986).
[22]A. Argiriou, M. Santamouris, and D. Assimakopoulos, "Assessment of the radiative cooling potential of a collector using hourly weather data," Energy **19**, 879–888 (1994).
[23]M. Hanif, T. Mahlia, A. Zare, T. Saksahdan, and H. Metselaar, "Potential energy savings by radiative cooling system for a building in tropical climate," Renewable Sustainable Energy Rev. **32**, 642–650 (2014).
[24]K. Zhang, D. Zhao, X. Yin, R. Yang, and G. Tan, "Energy saving and economic analysis of a new hybrid radiative cooling system for single-family houses in the USA," Appl. Energy **224**, 371–381 (2018).
[25]M. Li, Z. Liao, and C. F. M. Coimbra, "Spectral model for clear sky atmospheric longwave radiation," J. Quant. Spectrosc. Radiat. Transfer **209**, 196–211 (2018).
[26]M. Li, Z. Liao, and C. F. M. Coimbra, "Monte Carlo method for spectral solar irradiance on inclined surfaces," J. Renewable Sustainable Energy (unpublished) (2019).
[27]J. A. Duffie and W. A. Beckman, *Solar Engineering of Thermal Processes* (John Wiley & Sons, 2013).
[28]G. M. Hale and M. R. Querry, "Optical constants of water in the 200-nm to 200-μm wavelength region," Appl. Opt. **12**, 555–563 (1973).
[29]C. F. Bohren and D. R. Huffman, *Absorption and Scattering of Light by Small Particles* (John Wiley & Sons, 2008).
[30]J. E. Hansen and L. D. Travis, "Light scattering in planetary atmospheres," Space Sci. Rev. **16**, 527–610 (1974).
[31]N. L. Miles, J. Verlinde, and E. E. Clothiaux, "Cloud droplet size distributions in low-level stratiform clouds," J. Atmos. Sci. **57**, 295–311 (2000).
[32]H. Barker, G. Stephens, P. Partain, J. Bergman, B. Bonnel, K. Campana, E. Clothiaux, S. Clough, S. Cusack, J. Delamere *et al.*, "Assessing 1d atmospheric solar radiative transfer models: Interpretation and handling of unresolved clouds," J. Clim. **16**, 2676–2699 (2003).
[33]A. Walther, W. Straka, and A. Heidinger, *ABI Algorithm Theoretical Basis Document for Daytime Cloud Optical and Microphysical Properties (DCOMP), Version 2.0. NOAA/NESDIS* (Center for Satellite Applications and Research, 2011).
[34]M. Lee and R. O. Buckius, "Scaling anisotropic scattering in radiation heat transfer for a planar medium," J. Heat Transfer **104**(1), 68–75 (1982).
[35]M. Li, Y. Jiang, and C. F. M. Coimbra, "On the determination of atmospheric longwave irradiance under all-sky conditions," Sol. Energy **144**, 40–48 (2017).
[36]See https://www.ncdc.noaa.gov/data-access/land-based-station-data/land-based-datasets/automated-surface-observing-system-asos for "National Oceanic and Atmospheric Administration, Automated surface observing system (ASOS)."
[37]O. A. Alduchov and R. E. Eskridge, "Improved Magnus form approximation of saturation vapor pressure," J. Appl. Meteorol. **35**, 601–609 (1996).
[38]M. Tomczak, "Spatial interpolation and its uncertainty using automated anisotropic inverse distance weighting (IDW)-cross-validation/jackknife approach," J. Geogr. Inf. Decis. Anal. **2**, 18–30 (1998).
[39]See https://www.census.gov/geo/reference/gtc/gtc_census_divreg.html for "United States Census Bureau, Geographic terms and concepts - census divisions and census regions."